Spatiotemporal Evolution of Thin Liquid Films during Impact of Water Bubbles on Glass on a Micrometer to Nanometer Scale

Maurice H. W. Hendrix,[1,6] Rogerio Manica,[2,*] Evert Klaseboer,[2,†] Derek Y. C. Chan,[2,3,4,5,‡] and Claus-Dieter Ohl[6,§]

[1]*Physics of Fluids, University of Twente, P. O. Box 217, 7500 AE Enschede, The Netherlands*
[2]*Institute of High Performance Computing, 1 Fusionopolis Way, Singapore 138632*
[3]*Department of Mathematics and Statistics, University of Melbourne, Parkville 3010, Australia*
[4]*Faculty of Life and Social Science, Swinburne University of Technology, Hawthorn 3122, Australia*
[5]*Department of Mathematics, National University of Singapore, Singapore 119076*
[6]*School of Physical and Mathematical Sciences, Nanyang Technological University, Singapore 637371*

(Received 7 March 2012; published 15 June 2012)

Collisions between millimeter-size bubbles in water against a glass plate are studied using high-speed video. Bubble trajectory and shape are tracked simultaneously with laser interferometry between the glass and bubble surfaces that monitors spatial-temporal evolution of the trapped water film. Initial bubble bounces and the final attachment of the bubble to the surface have been quantified. While the global Reynolds number is large ($\sim 10^2$), the film Reynolds number remains small and permits analysis with lubrication theory with tangentially immobile boundary condition at the air-water interface. Accurate predictions of dimple formation and subsequent film drainage are obtained.

DOI: 10.1103/PhysRevLett.108.247803 PACS numbers: 68.15.+e, 47.55.nd, 47.15.gm, 47.55.dd

A key physical process that controls the impact of a bubble (or drop) on a solid-liquid interface is the drainage dynamics of the thin film trapped by the deformable object. The hydrodynamic drainage of this film down to the nm scale prior to rupture has a venerable history. In 1939, Derjaguin and Kussakov [1] demonstrated that when a macroscopic bubble is pushed towards a mica plate, the hydrodynamic pressure in the film not only flattens but can change the sign of the curvature of the bubble to form a dimple when the hydrodynamic pressure exceeds the bubble Laplace pressure. The characteristic time scale of the film drainage process depends on the boundary condition that pertains on the interfaces. In the low Reynolds number regime when inertia effects are small, the onset of dimple formation and the subsequent drainage of the liquid film trapped between a bubble and a wall [2,3], between a drop and a wall [4], and between two drops [5] occur on time scales on the order of seconds. Such phenomena have been modeled with quantitative precision [6]. On the other hand, the fast collision and attachment of millimeter-size bubbles in different fluids and on a variety of surfaces have been investigated experimentally by Zenit and Legendre [7], Malysa *et al.* [8], and Tsao and Koch [9]. The experiments are interpreted by treating the bubble as an effective particle whose deformation is analyzed in a phenomenological way. Quantitative theoretical analysis of fluid mechanics on the nanoscale remains elusive [10].

In this Letter, we report bubble impact experiments using direct high-speed (up to 54, 000 frames/s) video recordings, taken at two perspectives, of a millimeter-size bubble in water (0.5–1.5 mm diameter, Re ~50–230) colliding with a smooth glass surface. Trajectory data for the moving and deforming bubble are taken synchronously with laser interferometry recordings of the thinning of the water film trapped between the approaching bubble and the surface. Analysis of the interferometry fringes provides spatial-temporal information about the dynamic response of the water film down to a thickness of about ~100 nm. Although the film drainage process occurs on ms time scales, the Reynolds number based on the film thickness ($\sim \mu$m) remains small. This permits quantitative analysis with a lubrication model using a tangentially immobile hydrodynamic boundary condition at the bubble-water interface. Depending on the bubble size, the outcome of such interactions includes bubble bounces prior to final attachment to the surface. This study complements recent drop-impact studies in air [11], the impact and deformation of soap bubbles at the air-water interface [12] and the effect of a Leidenfrost vapor on the impact splash behavior of a drop on a hot surface [13].

A schematic of the experimental setup is presented in Fig. 1(a). A glass container (cross section: 4 by 4 cm, height: 20 cm) is filled with deionized water and covered with a glass microscope cover slip (Fisherbrand, thickness 0.17 mm). A bubble is released from a fine needle (Nordson EFD 32 G, inner diameter 0.10, outer diameter 0.24 mm) connected to a capillary at a distance of 5 mm below the glass surface. Upon release, it rises under buoyancy to reach terminal velocity before colliding with the glass cover slip. The bubble diameter can be varied between 0.5 to 1.5 mm by using a second precision syringe to inject an air bubble of controlled length into the capillary. Then, by pushing the first syringe the bubble is transported towards the needle tip until it is released gently into the water.

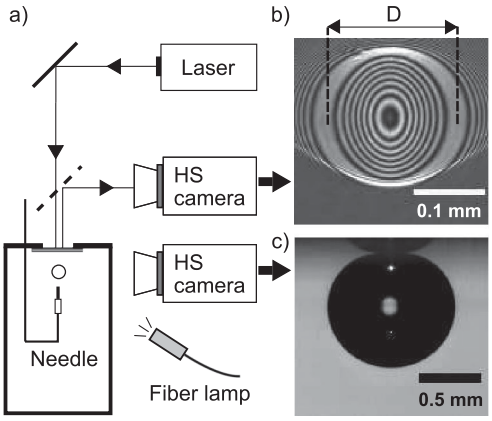

FIG. 1. (a) Schematic of the experimental setup. A bubble released from a fine needle rises towards the glass slide. Two synchronized high-speed cameras record the vertical bubble position and the interference fringes between the glass and the bubble surfaces. (b) A frame of the interferometric fringes from which the local film thickness h can be determined and the dimple diameter D is indicated. (c) Side view showing the bubble (radius $R_0 \approx 0.5$ mm) taken at the same time as the interference pattern, with a reflection at the glass surface.

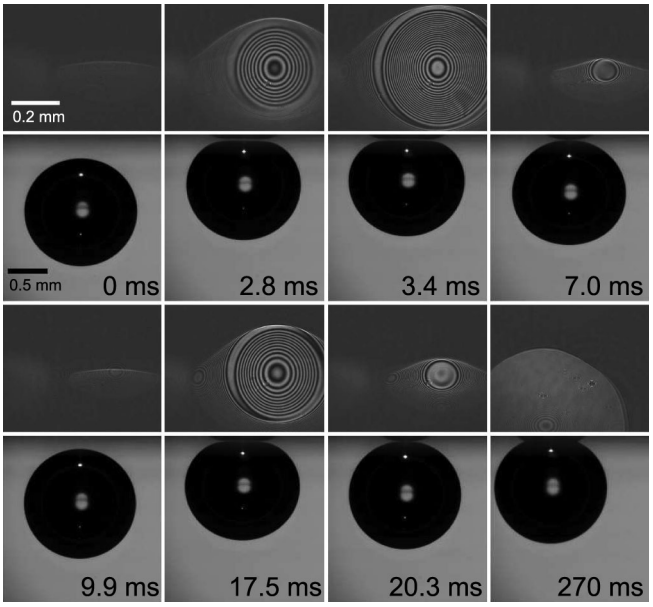

FIG. 2. The collision of a bubble of radius $R_0 \sim 690$ μm and terminal velocity $V_T = 14.8$ cm/s with the glass surface. The processes of bubble impact, dimple formation, bounce, and formation of three-phase contact line (see text) are evident.

For interferometry, a laser (2 mm beam diameter with 300 mW, Nd:YAG continuous wave laser, $\lambda = 532$ nm) after reflecting from a steering mirror is passed through a 50% beam splitter onto the glass slide at the area of bubble impact [Fig. 1(a)]. The interference pattern between light reflected from the glass-water and the bubble-water interface is recorded with a high-speed camera (SA1, Photron Inc.) at up to 54 000 frames/s through the beam splitter. A snapshot with a typical interference pattern is depicted in Fig. 1(b). A second high-speed (same frame rate) camera synchronized through a phased-locked-loop records a side view of the bubble rising and bouncing off the glass plate [Fig. 1(c)]. Such data furnished the bubble radius R_0 and the velocity of the center of mass $V(t)$ from the side view. Over 20 experimental runs have been recorded and analyzed.

In Fig. 2 we show a bubble of radius $R_0 = 0.69$ mm with terminal velocity of $V_T = 14.8$ cm/s. This gives a global Reynolds number of $Re = 2\rho R_0 V_T/\mu \approx 200$, where $\rho = 1000$ kg/m^3 is the density and μ the dynamic viscosity of water. The capillary number $\mathrm{Ca} = \mu V_T/\sigma$ is around 0.002, where $\sigma = 0.072$ N/m is the water surface tension. To describe our results, an arbitrary time origin $t = 0$ ms is set when the bubble still travels at a speed close to the terminal velocity and is barely deformed by the proximity to the glass surface. At $t = 2.8$ ms, the bubble has made "contact" with the glass, showing considerable deformation with a well-developed dimple. The circular symmetry of the fringes demonstrates that the trapped water film is axisymmetric. At $t = 3.4$ ms, the dimple has reached its maximum size while the deformation of the bubble is most pronounced. The bubble is about to reverse its trajectory and "separates" from the glass surface shortly after $t = 7.0$ ms. At time $t = 9.9$ ms, the bubble has receded furthest from the surface and is about to commence an approach for a second collision. The size of the dimple at the second encounter ($t = 17.5$ ms) is smaller due to the lower impact velocity. At this bubble size, the dimple resolves without further bounces. However, a small film is maintained ($t = 20.3$ ms) under buoyancy that forces the film to drain slowly. Eventually, the film ruptures at the dimple rim where the water film is thinnest and falls within the range of an attractive disjoining pressure that destabilizes the film. For all cases studied, we observe that the film rupture starts at the thinnest part of the water film located at the rim of the dimple. After rupture, a three-phase contact line forms and propagates until a final equilibrium state is attained at time $t = 270$ ms in Fig. 2 and results in a loss of interference fringes. All stages of the process can be clearly resolved and are now available for analysis.

The dewetting processes and the displacement of the water film by the three-phase contact line that formed after the film ruptured at the dimple rim is presented in Fig 3. Rupture breaks the axisymmetry of the film and the subsequent dewetting process is about 100 times faster than the film drainage process. This long film drainage time is called the induction time in the important particle-bubble pickup process central to mineral flotation; the very rapid dewetting process is relatively unimportant by comparison and is consistent with the coalescence of a mercury drop on to a mica surface under attractive electrical forces [14].

The collision and bounce of a bubble is characterized by the global Reynolds number ($\sim 10^2$) defined in terms of the bubble diameter and the terminal velocity. In contrast, the film drainage process is characterized by a small film

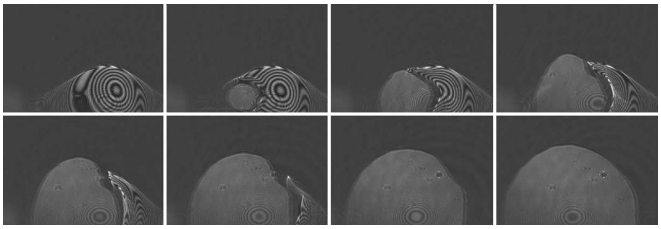

FIG. 3. The evolution of the dewetting process that corresponds to Fig. 2 with frames separated by 2.9 ms.

Reynolds number $\mathrm{Re}_f = \rho h_F V_F/\mu \ll 1$, where $h_F \ll R_0$ is the characteristic film thickness and V_F is the characteristic velocity of the air-water interface of the film. Therefore, the spatial-temporal evolution of the axisymmetric water film thickness, $h(r, t)$, can be described using lubrication theory. The hydrodynamic boundary condition at the glass surface is the usual tangentially immobile condition where the fluid velocity vanishes at the surface. Traditionally, the hydrodynamic boundary condition imposed at the air-water interface is the vanishing of tangential shear stress. However, this condition would predict film drainage rates that are 4 times faster than present experimental observations. On the other hand, imposing the tangentially immobile condition at the bubble surface gives excellent agreement with experiments without adjustable parameters. Surface contamination is responsible for this observation (see later).

With these boundary conditions, the film evolution is given by the Stokes-Reynolds equation $\partial_t h = 1/(12\mu r)\partial_r(rh^3\partial_r p)$. The fluid pressure p in the film, measured relative to bulk solution, is given by the Young-Laplace equation that depends on the curvature of the bubble-water interface $p + \Pi = 2\sigma/R - (\sigma/r)\partial_r(r\partial_r h)$. Here, $(2\sigma/R)$ is the Laplace pressure of the bubble with $R \sim R_0$ [15] and $\Pi(h)$ is the disjoining pressure that characterizes interactions between the glass surface and the bubble (e.g., van der Waals, electric double-layer interactions). This contribution is significant when the film thickness falls below about 100 nm and is responsible for initiating film rupture. To complete the model, we need one initial condition: $h(r, 0) = h_0 + r^2/2R_0$, where h_0 is some initial separation at which the deformation due to interaction is not important [at $t \sim -20$ ms in Fig. 4(a)] and four boundary conditions: $\partial_r h = 0 = \partial_r p$ at $r = 0$ due to symmetry, $p \sim r^{-4}$ as $r \to \infty$ [16] and at some large radial coordinate $r = r_{\max}$: $\partial_t h = -V(t)$, where $V(t)$ is the velocity of the center of mass of the bubble obtained from the experiment [see Fig. 4(a)].

We present a sample comparison, without adjustable parameters, for a smaller bubble ($R_0 = 385$ μm) with a lower terminal velocity so that it will not fully detach from the glass surface during rebound. Thus the fringe pattern is always present during the entire bubble-surface encounter. The order for the fringes is obtained from the point of film rupture. The position and velocity of the center of mass of the bubble, extracted from synchronized images of the side

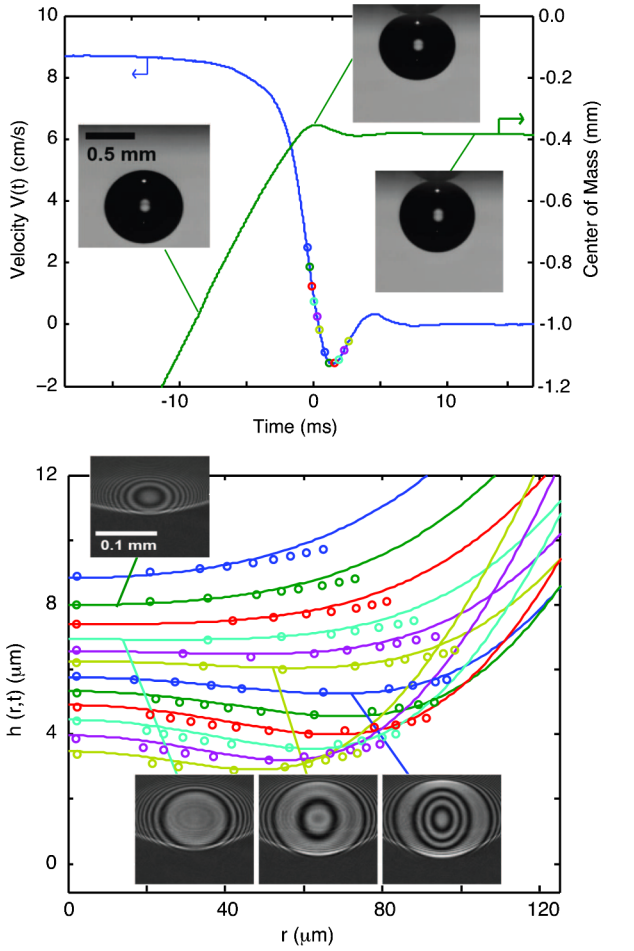

FIG. 4 (color online). (a) Measured time variations of the position and velocity of the center of mass of a bubble ($R_0 = 385$ μm) approaching the glass surface. Insets: Bubble shapes at the indicated time points. (b) Profiles of the film thickness at times t_i indicated by circles in part (a). Symbols denote experimental results, and solid lines represent our model with $V_T = 8.7$ cm/s. The first six film profiles are separated by 0.185 ms and the remaining are separated by intervals of 0.37 ms. Insets: Interference patterns at the indicated times.

view camera, provide the boundary condition data for our model.

In Fig. 4(a), we show the observed position and velocity of the bubble undergoing a gentle bounce. We define $t = 0$ to be the moment when the dimple first forms. Initially for $t \ll -10$ ms, the bubble approaches the surface with a constant terminal velocity of 8.7 cm/s. The presence of a bounce is indicated by the maximum in the center of mass position and the center of mass velocity changing sign at around $t = 0$. However, the bounce is gentle and the bubble remains sufficiently close to the surface to provide a continuously varying interference fringe pattern. In Fig. 4(b), we compare the measured film thickness during the bounce from the experiment (open circles) with the lubrication model (solid lines). We obtain excellent agreement in the position and time dependence between the model and experiments. In the insets selected interference

patterns are plotted. According to the model [5], a dimple forms at a separation of $h_D \approx 0.4R_0\sqrt{2\mathrm{Ca}} \sim 7\ \mu$m, which coincides with observations. A full video of this experiment together with trajectory data and calculated spatial-temporal evolution of the water film is available in the online Supplemental Material [17].

It is interesting to note that during the bounce, while the outer part of the bubble is retreating from the glass surface, the central portion of the film continues to thin. Similar behavior has been observed in the low Reynolds number experiments involving drop-surface [4], drop-drop [18,19], and bubble-bubble [20] encounters and is consistent with predictions from a perturbation analysis [21]. This observation suggests that although the (high Reynolds number) effect of inertia is central to the bounce phenomenon, the film drainage process appears to remain in the low Reynolds regime.

In earlier studies of the rise of 1.5-mm diameter bubbles in ultrapure water, the terminal velocity was found to be about 35 cm/s [8,22,23], provided an extreme level of cleanliness is maintained. However, the terminal velocity drops to around 15 cm/s with the addition of surfactants in parts per million concentration [8]. This effect has been attributed to adsorption of trace impurities at the bubble surface that generate sufficient Marangoni stress to render the bubble-water interface to behave like a solid surface with a tangentially immobile boundary. The terminal velocities of our comparable-sized bubbles are also $\sim$15 cm/s. We used deionized distilled water in our experiments and maintained normal levels of laboratory cleanliness, so it is possible that there is sufficient airborne contaminants under our laboratory conditions to render the bubble surfaces to be tangentially immobile. Indeed, the variation of terminal velocity of our bubbles with size ($50 < \mathrm{Re} < 250$) is found to be consistent with that predicted assuming a tangentially immobile boundary condition (see Supplemental Material [17]).

Using synchronized high-speed recordings to track bubble trajectory and the interference fringes generated by the thin water film trapped between the approaching bubble and the glass plate, we can accurately quantify bubble-surface collisions dynamics. Although the global Reynolds number of the approaching bubble is high, provided the motion of the bubble outside the film is available to furnish the required boundary condition, the spatial-temporal evolution of the thin water film can be described quantitatively by a low Reynolds number lubrication model that predicts the spatial-temporal evolution of the film radius and thickness with quantitative accuracy. Using the traditional zero tangential stress condition at the bubble surface would predict a much thinner water film and a drainage rate that is 4 times faster (see Supplemental Material [17]). The experiments resolved simultaneously the large scale center of mass movement and the microscopic thin film hydrodynamics. The excellent agreement between model and experiments attests that we have captured the essential physics of the bubble impact problem. Interestingly, the liquid-gas interfaces can support tangential stress, in agreement with similar studies in the low Reynolds number regime [15,20,24].

*manicar@ihpc.a-star.edu.sg
†evert@ihpc.a-star.edu.sg
‡D.Chan@unimelb.edu.au
§CDOhl@ntu.edu.sg

[1] B. Derjaguin and M. Kussakov, Prog. Surf. Sci. **40**, 26 (1992).
[2] L. R. Fisher, E. E. Mitchell, D. Hewitt, J. Ralston, and J. Wolfe, Colloids Surf. **52**, 163 (1991).
[3] R. A. Pushkarova and R. G. Horn, Colloids Surf. A **261**, 147 (2005).
[4] J. N. Connor and R. G. Horn, Faraday Discuss. **123**, 193 (2003).
[5] E. Klaseboer, J. P. Chevaillier, C. Gourdon, and O. Masbernat, J. Colloid Interface Sci. **229**, 274 (2000).
[6] D. Y. C. Chan, E. Klaseboer, and R. Manica, Soft Matter **7**, 2235 (2011).
[7] R. Zenit and D. Legendre, Phys. Fluids **21**, 083306 (2009).
[8] K. Malysa, M. Krasowska, and M. Krzan, Adv. Colloid Interface Sci. **114–115**, 205 (2005).
[9] H.-K. Tsao and D. L. Koch, Phys. Fluids **9**, 44 (1997).
[10] E. Klaseboer, J.-P. Chevaillier, A. Maté, O. Masbernat, and C. Gourdon, Phys. Fluids **13**, 45 (2001).
[11] J. Ruiter, J. M. Oh, D. van den Ende, and F. Mugele, Phys. Rev. Lett. **108**, 074505 (2012).
[12] F. Vincent, A. Le Goff, G. Lagubeau, and D. Quéré, J. Adhesion **83**, 897 (2007).
[13] T. Tran, H. J. J. Staat, A. Prosperetti, C. Sun, and D. Lohse, Phys. Rev. Lett. **108**, 036101 (2012).
[14] R. Manica, J. N. Connor, L. Y. Clasohm, S. L. Carnie, R. G. Horn, and D. Y. C. Chan, Langmuir **24**, 1381 (2008).
[15] D. Y. C. Chan, E. Klaseboer, and R. Manica, Adv. Colloid Interface Sci. **165**, 70 (2011).
[16] S. G. Yiantsios and R. H. Davis, J. Fluid Mech. **217**, 547 (1990).
[17] See Supplemental Material at http://link.aps.org/supplemental/10.1103/PhysRevLett.108.247803 for details on the terminal velocity, the effects of hydrodynamic boundary conditions, and the conversion of fringe intensities to film thickness. Additionally, a movie shows simultaneous views of the center of mass motion, film thickness, and interference fringe patterns during the collision event.
[18] N. Bremond, A. R. Thiam, and J. Bibette, Phys. Rev. Lett. **100**, 024501 (2008).
[19] D. Z. Gunes, X. Clain, O. Breton, G. Mayor, and A. S. Burbidge, J. Colloid Interface Sci. **343**, 79 (2010).
[20] I. U. Vakarelski, R. Manica, X. Tang, S. J. O'Shea, G. W. Stevens, F. Grieser, R. R. Dagastine, and D. Y. C. Chan, Proc. Natl. Acad. Sci. U.S.A. **107**, 11177 (2010).
[21] D. Y. C. Chan, E. Klaseboer, and R. Manica, Soft Matter **5**, 2858 (2009).
[22] P. C. Duineveld, J. Fluid Mech. **292**, 325 (1995).
[23] E. Klaseboer, R. Manica, D. Y. C. Chan, and B. C. Khoo, Eng. Anal. Bound. Elem. **35**, 489 (2011).
[24] R. R. Dagastine, R. Manica, S. L. Carnie, D. Y. C. Chan, G. W. Stevens, and F. Grieser, Science **313**, 210 (2006).